Proceedings of ASME Turbo Expo 2011
GT2011
June 6-10, 2011, Vancouver, British Columbia, Canada

GT2011-46289

EXPERIMENTAL INVESTIGATION OF FORCED RESPONSE IMPELLER BLADE VIBRATION IN A CENTRIFUGAL COMPRESSOR WITH VARIABLE INLET GUIDE VANES - PART 1: BLADE DAMPING

Armin Zemp*
Reza S. Abhari
LEC, Laboratory for Energy Conversion
Department of Mechanical and Process Engineering
ETH Zurich, Switzerland
e-mail: zemp@lec.mavt.ethz.ch

Beat Ribi
MAN Diesel & Turbo AG Schweiz
Zurich, Switzerland

ABSTRACT

Forming the first part of a two-part paper, the quantification of the resonant response levels and the damping quantities for a centrifugal compressor impeller with variable inlet guide vanes under engine representative operating conditions is detailed in this work. The motivation for the investigation is the lack of experimental data that are needed to improve and validate computational tools used during the design phase. Measurements were performed during resonant blade vibrations with the inlet pressure, the inlet guide vane angle and the operating point as the varying parameters. The flow non-uniformity introduced into the inlet flow field was measured with an aerodynamic probe. These measurements showed an increase in flow distortion for increased guide vane angles. The response amplitudes were acquired with dynamic strain gauges. A curve-fit method was applied to estimate the critical damping ratios. The results showed a linear correlation of the aerodynamic damping with the inlet pressure. The mode dependent material damping was therefore derived using a linear extrapolation to vacuum conditions of the inlet pressure dependent overall damping. The resonant blade dynamics could be captured with a single degree of freedom model. The aerodynamic damping and the maximum strain response were found to significantly depend on the inlet guide vane angle setting and on the throttle setting of the compressor.

*Address all correspondence to this author.

NOMENCLATURE

c	viscous damping coefficient	$[Ns/m]$
C	velocity in absolute frame of reference	$[m/s]$
CFD	computational fluid dynamics	
EO	engine order	
F, F_0	forcing function, force amplitude	$[N]$
$F_V, F_{V,M}, F_{V,A}$	damping force, material, aerodynamic	$[N]$
f	frequency	$[Hz]$
FSI	fluid structure interaction	
h	blade height at leading edge	$[mm]$
H	enthalpy	$[J/kg]$
IGV	inlet guide vane	
k	spring constant	$[N/m]$
m	mass	$[kg]$
Mu	stage Mach number	
OL	operating line	
p	pressure	$[Pa]$
Q	corrected mass flow rate	$[-]$
S_{max}	maximum sweep rate	$[Hz/s]$
$SDOF$	single degree of freedom	
t	time	$[s]$
U	blade speed	$[m/s]$
V	velocity	$[m/s]$
$\dot{V}$	volumetric flow rate	$[m^3/s]$
$VIGV$	variable inlet guide vane	
$x, \dot{x}, \ddot{x}$	displacement, speed, acceleration	$[m, m/s, m/s^2]$

Greek:

ε	strain	[%]
ϕ_0	phase angle	[°]
π	pressure ratio	[−]
ζ	critical damping ratio	[−]
ω	frequency in radians	[$^{rad}/_{s}$]
ω_n	natural frequency in radians	[$^{rad}/_{s}$]
γ	IGV angle (relative to axial)	[°]

Subscripts:

ax	in axial direction
M,A	material, aerodynamic
ref	reference quantity
res	at resonance
Θ	in circumferential direction
0	total quantity
1	at compressor inlet
2	at compressor outlet

INTRODUCTION

In turbomachinery applications, depending on the operating conditions and the flow properties, the blades suffer from flutter and/or forced response blade vibrations. These blade vibrations are caused, amongst other reasons, by unsteady fluid structure interactions as conditioned by duct bends, struts or by rotor-stator interactions.

The reliable prediction of the vibratory response of the structure during the design phase is essential to guarantee the mechanical integrity of each of the components. Correct assessment necessitates the quantification of the excitation amplitudes and the damping properties under engine representative operating conditions. These parameters are needed as an input for numerical models to predict the vibratory response levels in the design phase. A quantification of the costs generated in this field during the design process and due to operational failures is given in the frequently cited publications by *El-Aini et al.* [1] and *Kielb* [2]. The overall blade damping which is generally composed of material, mechanical and aerodynamic damping, depends on the associated blade properties, i.e. the material properties, the blade attachment, the blade design and the operating conditions. A summary of the different experimental approaches and the problem modeling was presented by *Srinivasan* [3,4].

In the past, researchers generally focused on the estimation of mechanical damping, as this is the damping property that can be directly influenced by the designer. The material damping was basically assumed to be insignificant and was therefore neglected during the design phase as noted by *Srinivasan et al.* [5]. However, for unshrouded centrifugal compressor impellers, where the impeller is machined from one single piece, the mechanical damping is also assumed to be insignificant. Therefore, aerodynamic damping can be regarded as the dominant damping mechanism for centrifugal compressor blades.

Only very limited data on aerodynamic damping is available for rotating blades under engine representative operating conditions showing the sensitivity of the damping properties on different parameters and it focuses mainly on axial machines. *Crawley* [6] presented experimentally estimated aerodynamic damping properties for a transonic compressor with a distorted inlet flow field. The importance of experimental research in the field of forced response for a fan under engine representative conditions was presented in detail by *Manwaring et al.* [7–10]. The experiments quantified the effect of the inlet flow conditions and the blade pressure distribution on the vibratory response of the blades. The results were used to improve the numerical tools used during the design phase of the blades. Experimental research in this field for centrifugal compressors was performed by *Haupt and Rautenberg* [11] and supplemented by *Jin* [12]. The investigations focused on an improved understanding of the excitation mechanisms for stable and unstable compressor operating conditions. In test rigs where the inlet pressure can be set, the aerodynamic damping is obtained by subtracting the non-aerodynamic damping, measured at vacuum conditions, from the estimated overall damping. This approach was used by *Kielb and Abhari* [13] to separate the different damping contributions in their experiments on a full-scale rotating turbine. The recently published papers by *Kammerer and Abhari* [14,15] present an experimental approach to estimate blade damping in a high-speed centrifugal compressor under different operating conditions. Their results showed the influence of the inlet pressure and the operating point on the damping properties for the first and second main blade modes. The resonant blade response was achieved by the installation of distortion screens in the inlet section of the centrifugal compressor test rig.

Parallel to the experimental work, the computation of the unsteady flow and the structure can be performed to calculate the aerodynamic damping and the strain distribution within the structure. Generally, there are two different approaches. The fluid and the solid domains can be fully coupled or they can be treated as two separate domains. In the case of two decoupled domains, the overall damping is required as an input for the calculation and therefore has to be experimentally estimated. *Abhari and Giles* [16] presented a numerical approach to successfully predict the motion-dependent aerodynamic damping for oscillating airfoils in a cascade. A computational method to include the influence of neighboring blade rows on the aerodynamic damping of a cascade of vibrating blades was presented by *Silkowski and Hall* [17]. *Dickmann et al.* [18] presented a fluid structure interaction calculation for a decoupled system of a centrifugal compressor stage.

MOTIVATION AND SCOPE OF THE PAPER

The aim of this paper is to present and discuss experimental results for forced response blade vibration measurements for a centrifugal compressor with variable inlet guide vanes. This experimental investigation was motivated by the need for reliable and engine representative data to advance understanding of forced response blade vibrations of centrifugal compressor impellers and the development and validation of computational tools required for the design process. In Part 1 of this two-part publication the scope was to detail the influence of the inlet pressure, the inlet guide vane angle setting and the operating point (near-choke, design point and near-stall) on the measured blade strain amplitudes and damping properties.

In the second part of this two part publication [19] the investigation focused on the evolution of the forcing function. The change in the unsteady blade pressure distribution was measured with blade-mounted fast-response pressure sensors. The measurements allowed the quantification of the amplitude and phase angle and a comparison with numerical predictions from 3D unsteady CFD calculations. Finally, the experimentally estimated damping properties and unsteady blade pressure distributions from the calculations were used as an input for a unidirectional FSI calculation. The predicted strain levels were compared with experimental values. The requirements and limitations of unidirectional FSI calculations could be demonstrated.

TEST FACILITY AND EXPERIMENTAL APPROACH

Test Facility

The experiments were performed in a single-stage centrifugal compressor rig at the Laboratory for Energy Conversion at the Swiss Federal Institute of Technology in Zurich, Switzerland. A schematic drawing of the test facility is shown in figure 1. The rig is operated in a closed loop arrangement. This allows adjustment of the inlet pressure and temperature independently of ambient conditions. In this work, the inlet pressure was varied from 0.2 bar to 0.8 bar absolute. The impeller is driven by a 440 kW DC motor with a two-stage gearbox. The maximum shaft speed is limited to 22'000 rpm. At the compressor inlet, the temperature as well as the pressure are measured and can be held constant at the requested values by a control system. Downstream of the compression stage, the working fluid is cooled by a heat exchanger and discharged with a throttle device. The throttle is also used to set the requested mass flow rate. The mass flow is measured with a standard orifice downstream the throttle. The performance of the compressor is estimated by the measurement of temperatures and pressures upstream and downstream of the compression stage. The impeller used in this investigation has an outer diameter of 400 mm and features 7 main and 7 splitter blades. The design total pressure ratio is $\pi_0 = 2.8$ at a design volumetric flow rate of $\dot{V} = 3.5\ m^3/s$.

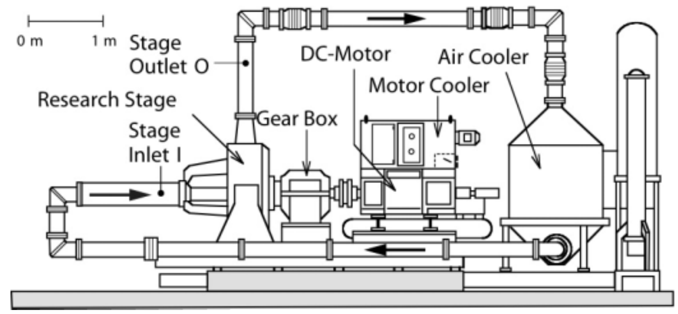

FIGURE 1. Centrifugal Compressor Test Facility

A detailed description of the impeller design is given by *Schleer* [20]. Downstream of the impeller is a parallel and vaneless diffuser with an exit diameter of 580 mm and a diffuser channel height of 15.8 mm. The diffuser flow is discharged into a toroidal collecting chamber.

Variable Inlet Guide Vanes in Centrifugal Compressors

Centrifugal compressors in industrial applications can be required to operate over a wide range of mass flow rates at constant pressure ratios with constant rotational speeds. This can be achieved by the integration of a variable inlet guide vane ($VIGV$) row that induce a controlled inlet pre-swirl. The use of variable inlet guide vanes in a centrifugal compressor not only allows for adjustment of the rotor inflow properties, but also enables the reduction in the required power for starting up the compressor. The influence of the pre-swirl on the performance of the machine has been studied by *Traupel* [21].

The integration of upstream components of a centrifugal compressor stage such as inlet guide vanes unavoidably introduces flow field distortions. Detailed measurements downstream of an inlet guide vane row were carried out by *Kassens and Rautenberg* [22]. These flow non-uniformities potentially cause fluid structure interactions with the impeller blades and are therefore a possible source of forced response impeller blade vibrations.

Experimental Approach

The goal of this work was to quantify the damping ratios and strain rates for impeller blade forced response vibrations caused by inlet flow non-uniformities introduced by a row of variable inlet guide vanes. The contributions of material and aerodynamic damping to the overall damping were separated at different op-

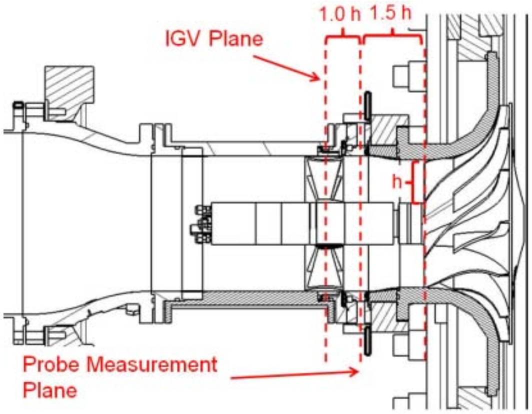

FIGURE 2. Experimental Setup within the Suction Pipe

erating conditions of the compressor. Figure 2 shows the experimental setup in the inlet section of the test rig. The main components of the setup are the inlet guide vanes, the rotary transmitter, the instrumented impeller and the access for aerodynamic probe measurements downstream of the IGV row. The $VIGV$s are 2.5 impeller blade heights upstream of the impeller eye. The aerodynamic probe measurement plane is 1 blade height downstream of the $VIGV$ row and 1.5 blade heights upstream of the impeller eye. It was necessary to measure the distorted flow upstream of the impeller in order to visualize and quantify the amount of flow non-uniformity introduced into the flow for the different IGV blade angle and mass flow settings. The measured flow properties were also needed as inlet boundary conditions for the 3D unsteady CFD calculations in Part 2. The rotary transmitter in the center of the suction pipe was required to transfer the signals from the dynamic strain gauges mounted on the blade surfaces to the data acquisition system.

FIGURE 3. Interchangeable Inlet Guide Vane Row

The blade geometry of the inlet guide vane was a scaled blade shape used by one of the industrial partners for the current research project. The $-30°$ configuration of the interchangeable inlet guide vane row is shown in figure 3. The inlet guide vane row featured 12 vanes. The number of blades was adjusted to the centrifugal test rig shaft speed range and to the modal properties of the impeller blades in use in order to provoke a resonance condition within the available speed range. The Campbell diagram for the impeller main blade shown as figure 4, shows the resonant crossing at about 6500 rpm for mode 1 with $EO12$.

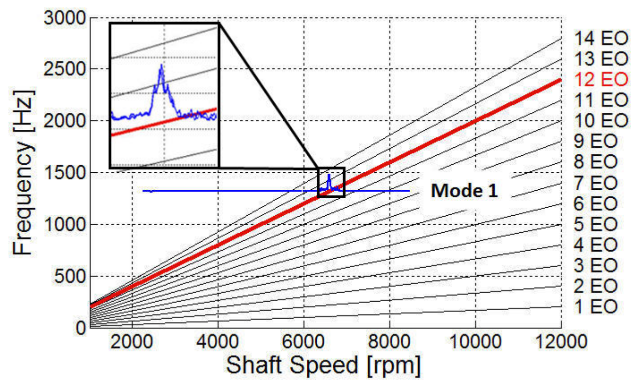

FIGURE 4. Campbell Diagram for the Impeller Main Blade

Flow Field Measurement Downstream of the IGV

A miniature pneumatic four-hole probe was used to measure the 3D steady flow properties downstream of the inlet guide vanes. The cylindrical probe has a calibration range of $\pm 30°$ in yaw and $\pm 24°$ in pitch angles. The probe tip diameter is 1.8 mm. A detailed summary of the probe properties has been given by *Lenherr et al.* [23]. The probe was mounted on a traversing system which enabled the automatic positioning of the probe head in radial as well as in circumferential directions. The results from the probe measurements of the non-uniform flow field downstream of the IGV will be presented in the results section.

Blade Strain Measurement Procedure and Modeling

The expected stress levels due to the resonant blade vibrations were assumed to be high enough to cause a blade failure after a certain number of vibration cycles. Therefore, a transient measurement approach was used to pass the resonant speed range. The measurements were done with a constant shaft speed sweep rate according to *Ewins* [24], in order to achieve a quasi-steady state blade response.

$$S_{max} = 3.6\, f_{res}^2\, \zeta^2 \left[\frac{\text{Hz}}{\text{s}}\right] \quad (1)$$

Vibratory stresses were measured with dynamic strain gauges applied onto the blade surfaces. Each main blade was equally instrumented with one strain gauge. The positioning of the strain gauges was optimized to capture the response of the first two main blade eigenmodes using the procedure presented by *Szwedowicz et al.* [25]. A slip ring was used to transmit data to the data acquisition system. Each data channel was scanned with a sampling rate of 200 kHz. A reference one-per-revolution signal was used to track the rotational speed.

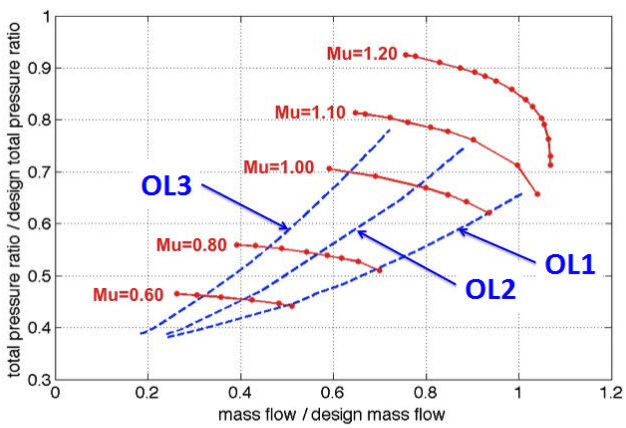

FIGURE 5. Compressor Map and Operating Lines

In this paper results will be compared between three different throttle settings corresponding to operating line 1 (*OL*1), *OL*2 and *OL*3, see figure 5. *OL*1 corresponds to a near-choke condition, *OL*2 to a realistic operational setting and *OL*3 to a near-stall condition.

For centrifugal impeller blades, as used in this investigation, mechanical damping was neglected due to the lack of component friction. Damping during resonant vibration is therefore only provided through material and aerodynamic damping. In the following, damping will be mathematically accounted for by the critical damping ratio ζ according to a vibrating single degree of freedom (*SDOF*) system with viscous damping. The *SDOF* system can be described by the differential equation of the form:

$$m\ddot{x} + c\dot{x} + kx = F(t) \quad (2)$$

with x as the blade displacement. The time dependent force $F(t)$ is assumed to be of the form:

$$F(t) = F_0\, cos[2\pi f(t)t + \phi_0] \quad (3)$$

where the frequency sweep $f(t)$ is modeled using the relation:

$$f(t) = \frac{1}{2}\beta t + f_0 \qquad \text{with} \qquad \beta = \frac{f - f_0}{t - t_0} \quad (4)$$

The frequency as a function of time represents the constant impeller sweep rate during the experiments. The solution of the differential equation can be numerically obtained through interpolation of the excitation function and employment of the linear response of a *SDOF* system to step excitation. Details on this procedure can be found in *Craig and Kurdila* [26].

The overall viscous force F_V acting on the structure is expressed by:

$$F_V = -c\dot{x} = -2\zeta m\omega_n\dot{x} \qquad \text{with} \qquad \zeta = \frac{c}{2\omega_n m} \quad (5)$$

The total viscous force F_V is the sum of the material and aerodynamic damping forces $F_{V,\,M}$ and $F_{V,\,A}$:

$$\begin{aligned} F_V &= F_{V,\,M} + F_{V,\,A} & (6)\\ &= -2\zeta_M m\omega_n\dot{x} + F_{V,\,A} & (7)\end{aligned}$$

In equation 7, ζ_M is the critical damping ratio due to material damping. Material damping in the present work is assumed to be constant. The damping force due to aerodynamic damping is dependent on the density and therefore the inlet pressure was one parameter which was varied in this investigation. Scaling the aerodynamic damping force with inlet pressure, the following can be stated:

$$\begin{aligned} F_{V,\,A} &= F_{V,\,A,\,ref}\left(\frac{p}{p_{ref}}\right) & (8)\\ &= -2\zeta_{A,ref}\left(\frac{p}{p_{ref}}\right) m\omega_n\dot{x} & (9)\end{aligned}$$

And therefore, the overall damping can be derived as a function of the inlet pressure:

$$F_V = F_{V,\,M} + F_{V,\,A} \tag{10}$$

$$-2\zeta m\omega_n\dot{x} = -2\zeta_M m\omega_n\dot{x} - 2\zeta_{A,ref}\left(\frac{p}{p_{ref}}\right) m\omega_n\dot{x} \tag{11}$$

$$\zeta = \zeta_M + \zeta_{A,ref}\left(\frac{p}{p_{ref}}\right) \tag{12}$$

At vacuum conditions, assuming aerodynamic damping to be negligible, material damping is the only contributor to vibratory energy dissipation. The material damping can be experimentally estimated by measuring the overall damping at different inlet pressure settings and then extrapolating the values to zero inlet pressure. The critical damping estimation was performed using a curve fit method as described in detail by *Kammerer and Abhari* [15]. Finally, the maximum response during resonant vibration of the *SDOF* system can be represented as:

$$x = \frac{\frac{1}{k}F_{ref}\left(\frac{p}{p_{ref}}\right)}{2\left(\zeta_M + \zeta_{A,ref}\left(\frac{p}{p_{ref}}\right)\right)} \tag{13}$$

RESULTS

In the following sections results are presented for experimental investigations at different compressor operating points, at various compressor inlet pressures and for varied inlet guide vane angle settings. These three parameters were independently investigated to separate the effects on the overall performance of the compressor and its influence on the vibratory blade response and the damping quantities. It is important to mention that the results presented in the following focus on the forced response of the impeller main blades for the resonant crossing of blade mode 1 with its fundamental excitation (*EO*12). The compressor inlet pressure was varied from 0.2 bar to 0.8 bar absolute. Results for three different inlet guide vane angle γ settings (0°, $-30°$ and $-45°$) will be discussed in this paper. The negative blade angle indicates a pre-swhirl in a counter direction to the impeller rotation.

Influence of IGV Angle on Impeller Inlet Flow Properties and Compressor Performance

The introduced pre-swirl significantly influenced the work input coefficient of the centrifugal compressor stage. The Euler Turbine Equation directly relates the amount of pre-swirl with the total enthalpy rise over the stage. The direction of the pre-swirl in the present investigation was in the opposite direction to the impeller rotation and therefore the entropy rise over the stage was increased with larger negative inlet guide vane angles γ.

This implies that it would be necessary to decrease the blade tip speed to maintain the same level of impeller pressure ratio as was obtained without pre-swirl. However, as the present investigation focused on the blade resonant response the blade tip speed of interest is constant.

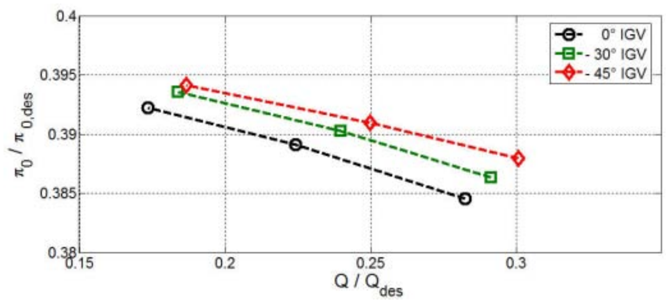

FIGURE 6. Compressor Map at Resonant Shaft Speed

Therefore, as the negative *IGV* angle γ increased, the compressor performance in terms of total pressure ratio π_0 increased at constant shaft speed. Figure 6 shows the measured performance at the shaft speed where the resonant crossing for the impeller main blade with the fundamental excitation order occurred. As expected, the curves not only show an increased pressure ratio but also that the performance map of the stage shows the trend of shifting to the larger flow rate with increased negative *IGV* angle.

The results of the pneumatic probe measurements downstream of the inlet guide vane row not only allowed quantification of the amount of distortion introduced to the inlet flow field as a function of the *IGV* angle, but can also be used to visualize the change in the shape of the low momentum fluid zone in the wake region of the blades. In figure 7, the normalized absolute Mach number $Ma_{abs}/Ma_{abs,mean}$ is plotted for three different *IGV* angles γ at a constant corrected mass flow ratio $Q/Q_{des} = 0.48$. The 0° *IGV* formed a straight low momentum wake over the whole flow channel height. The velocity deficit in the wake region was about 10% below the mass flow averaged mean value for the corrected mass flow ratio Q presented. The low momentum zone for the $-30°$ case showed an increased extent in circumferential direction and the velocity deficit increased to values of about 25% below the mean Mach number downstream of the inlet guide vane row. In the tip region the low momentum wake mixed out driven by the high amount of swirl in the flow field. This effect was even more pronounced in the $-45°$ case. The measurement showed only a small rudiment of the blade wake in the near hub region and up to about 50% *IGV* span.

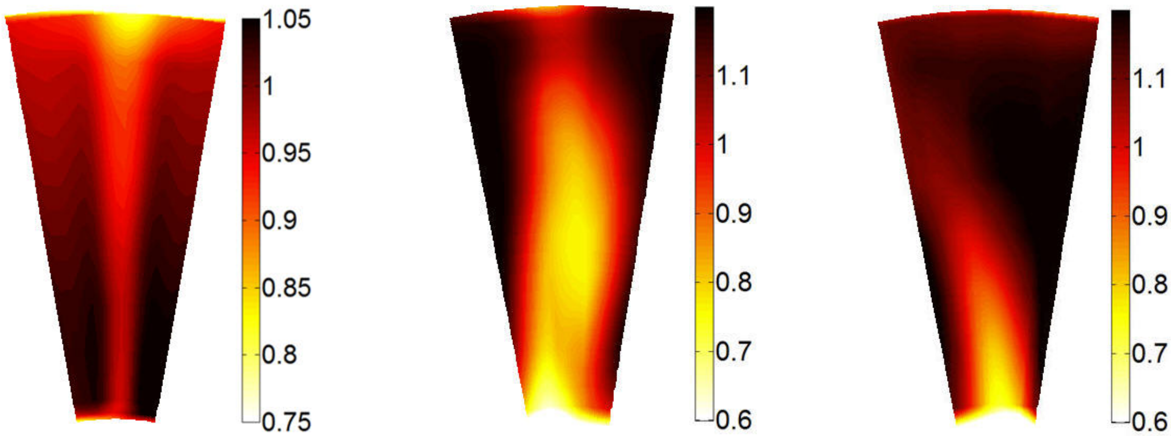

(a) 0° IGV Angle (b) $-30°$ IGV Angle (c) $-45°$ IGV Angle

FIGURE 7. Measured Normalized Absolute Mach Number $Ma_{abs}/Ma_{abs,mean}$ at $Q/Q_{des} = 0.48$

Over the whole range, the Mach number in the free stream region increases with increased *IGV* blade angle as expected due to the increased swirl. Up to $\gamma = -30°$ the Mach number in the wake region of the *IGV* decreased and therefore the inlet flow distortion increased. But for $\gamma = -45°$ the wake region shows higher absolute Mach numbers compared to the $\gamma = -30°$ case. The enhanced mixing and the increased flow path length for the swirling flow are the reasons for the reduction of the inlet flow distortion.

Influence of Inlet Pressure on Strain Response and Blade Damping

Inlet pressure is one parameter that directly influences the response amplitude and the damping of the impeller blades. Therefore, the experiments were performed for a number of inlet pressure settings. The inlet pressure setting not only affects the unsteady load but also influences the critical damping ratio, as both quantities scale with the density. The unsteady loading acting on the blade surface depends on the pressure difference between pressure and suction sides. The pressure differences scale with the inlet pressure and therefore scale the unsteady forces that cause the resonant response.

The main contributor to blade damping in a centrifugal compressor is aerodynamic damping. The aerodynamic damping is the result of the vibratory blade motion and the resultant unsteady force acting on the blade. Therefore, as this force depends on the unsteady pressure distribution, the aerodynamic damping scales with the inlet pressure as well.

Figure 8 shows the dynamic response of a blade during a transient measurement. The inlet pressure for the presented

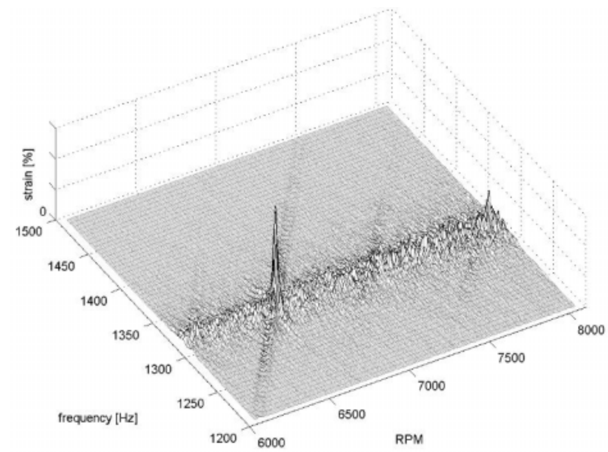

FIGURE 8. Mode 1 Response for EO12 Excitation at 0.8 bar and $-30°$ *IGV* Angle

response was set at 0.8 bar. The inlet guide vane angle γ was set at $-30°$. The traces of the first eigenfrequency as well as of the *EO*12 excitation could clearly be identified over the whole shaft speed range. The resonant response occured at about 6600 rpm.

Figure 9 shows the maximum response amplitude of the blades for different inlet pressure settings. The error bars indicate the variation of the response amplitude between the seven blades. The curve for the *SDOF* model was calculated according to equation 13 using the measured damping properties. The sufficiently good match between the model and the experimental values confirmed the use of a *SDOF* model to represent the blade dynamics during resonant vibration.

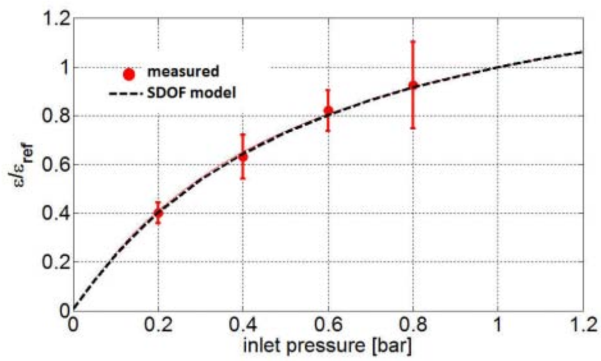

FIGURE 9. Strain Amplitude versus Inlet Pressure, *OL*2, $-30°$ *IGV* Angle

The corresponding damping ratios are shown in Figure 10. According to the derived correlation between the inlet pressure and the critical damping ratio in equation 12, Figure 10 shows the linear increase in critical damping ratio with increased inlet pressure. The error bars again show the variation for the seven impeller main blades.

Two observations could be made concerning the influence of the inlet pressure on the structural response and the damping ratio. Firstly, the strain amplitude showed an asymptotic behavior with increased inlet pressure. Therefore, the contribution of the material damping to the overall damping could be assumed to decrease with increasing inlet pressure. As a consequence, at a certain inlet pressure, the increases in excitation as well as the aerodynamic damping become almost equal. Secondly, the contribution from aerodynamic damping to the overall damping was in the same order of magnitude. At 1 bar inlet pressure the aerodynamic damping would be about 3 times higher than the material damping.

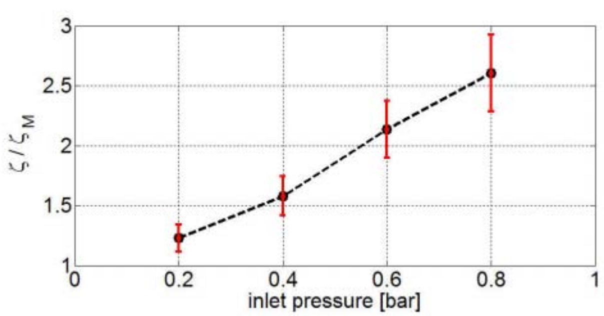

FIGURE 10. Critical Damping Ratio versus Inlet Pressure, *OL*2, $-30°$ *IGV* Angle

Compared to the aerodynamic damping estimation presented by *Kammerer and Abhari* [15] the contribution from aerodynamic damping to the overall damping is a factor of 3 smaller in the present investigation. The reason for the reduction in the aerodynamic damping was on one hand the reduced compressor mass flow at the resonant shaft speed for the *EO*12 excitation compared to the *EO*5 inlet flow distortion in the experiment of *Kammerer and Abhari* [15] and on the other hand the change in the circumferential spatial extent of the distortion pattern. The comparatively narrow circumferential extent of the low momentum fluid region downstream of the inlet guide vane may affect the aerodynamic work done from the fluid on the blades and vice versa; this hypothesis is being assessed in ongoing analysis of on-blade pressure measurement data. Nevertheless, the above observations clearly indicate that it is imperative to perform the damping estimation under engine representative operating conditions.

Influence of IGV Angle on Strain Response and Blade Damping

In this work, results for three different *IGV* angle settings are presented to detail the influence on the maximum strain amplitudes and on the damping quantities. Figure 11 shows the different resonant response amplitudes, $\varepsilon/\varepsilon_{ref}$, for the $0°$, $-30°$ and the $-45°$ *IGV* settings. The characteristics showed the same inlet pressure dependency as already discussed for figure 9. All three curves for the different *IGV* angles γ converged to $\varepsilon/\varepsilon_{ref} = 0$ for vacuum conditions. They also showed an asymptotic approximation to a strain level where the contribution of the material damping to the overall damping becomes insignificant. The important finding in this diagram was the fact that the strain response didn't grow with increased *IGV* angle γ. There was an increase in resonant response for $\gamma = -30°$ compared to the $0°$ setting by about 20% to 30%. However, the $-45°$ configuration showed the lowest strain rates. The measured amplitudes were about 10% to 15% below the values for the $\gamma = 0°$ configuration.

The reason for the observed reduction is the reduced amount of distortion introduced into the inlet flow field as illustrated in figure 7 and therefore a lower forcing of the impeller blades for the $-45°$ *IGV* blade angle configuration.

The comparison of the damping ratios showed lowest critical damping ratios for the $0°$ *IGV* angle setting γ and an increase with an increased blade angle setting. The three curves in Figure 12 all converged to a ratio $\zeta/\zeta_M = 1$ at vacuum conditions. All configurations scaled linearly with increased inlet pressure but the characteristics showed a different slope. The difference in the critical damping ratios for the distinct blade angle settings can be neglected at low inlet pressures below 0.2 bar. The second part of this two-part publication focused on the forcing functions

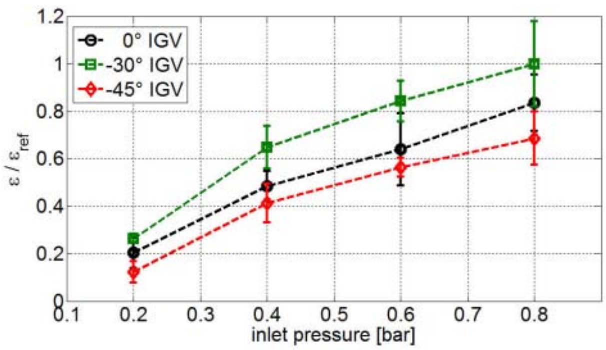

FIGURE 11. Strain Amplitude versus IGV Blade Angle γ, $OL2$

for the different IGV configurations. The unsteady blade pressures were measured with blade-mounted fast-response pressure sensors. The measured amplitudes as well as the phase angles were compared with 3D unsteady CFD calculations.

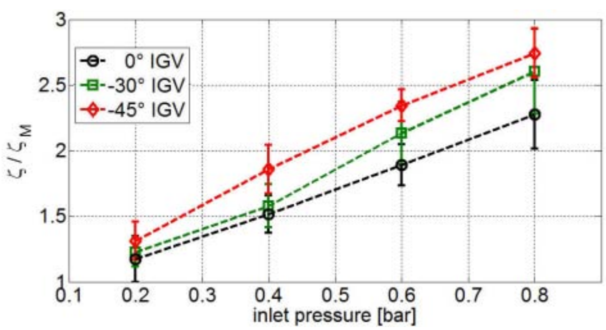

FIGURE 12. Critical Damping Ratio versus IGV Blade Angle γ, $OL2$

Influence of Operating Line on Strain Response and Blade Damping

The three different operating lines $OL1$ near-choke, $OL2$ at a design point setting and $OL3$ near-stall also influenced the response and damping characteristics of the impeller main blade as illustrated in figure 5. In the following section the influence of the operating point on the resonant response amplitudes and on the damping quantities will be discussed. Figure 13 compares the strain rates for the three different mass flow settings. The close to choke condition, $OL1$, showed 40% to 50% higher response amplitudes for all the inlet pressure values. The amplitudes for $OL2$ (design point) and $OL3$ (near-stall) were in a comparable range, with slightly higher values for the near-stall condition. The error bars indicate a decrease in the blade to blade variation for the operating line close to choke. Generally, the deviation increased at higher inlet pressure settings except for $OL1$, where the variation between the seven blades was smaller than in the other two cases.

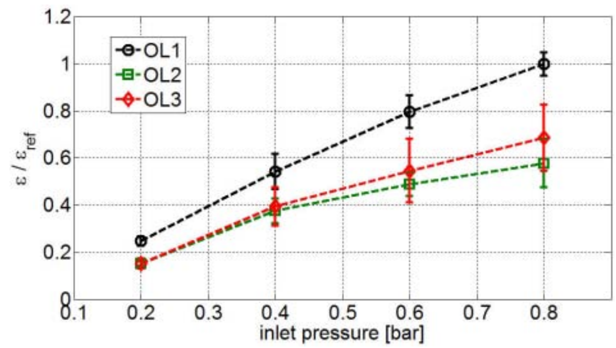

FIGURE 13. Strain Amplitude for Different Operating Lines, -30° IGV Angle

The corresponding critical damping ratios, as shown in figure 14, showed one reason for the decreased strain levels for $OL2$ compared to $OL3$. The critical damping ratios were higher compared to the near-stall operating condition, and therefore the increased damping reduced the response amplitudes. Although the near-choke conditions showed the highest damping quantities, this operating condition exhibited the highest strain amplitudes. The reason for the increased vibratory response level at near-choke conditions was a stronger forcing of the blade vibration during resonance. The detailed investigation of the forcing functions is presented in Part 2.

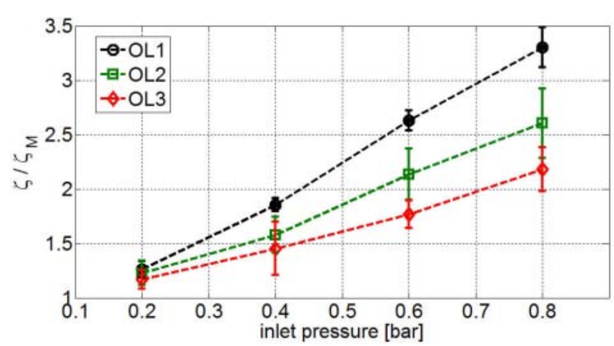

FIGURE 14. Critical Damping Ratios for Different Operating Lines, -30° IGV Angle

Combined Effects of Inlet Pressure, IGV Angle and Operating Point on Strain Response and Blade Damping

According to the results presented in the previous subsections there are two extreme cases with respect to maximum response amplitudes and critical damping ratios.

Generally, the critical damping ratio is linearly scaled with the inlet pressure if the compressor operating point and the inlet guide vane angle are kept constant. Therefore, the maximum damping rates were obtained at the highest inlet pressures and vice versa.

Larger negative inlet guide vane angles γ increased the aerodynamic damping, as shown in figure 12, and the blade loading decreased the aerodynamic damping ratios as illustrated in figure 14.

The strain levels did not show similar trends as the forcing function for the $-45°$ *IGV* configuration showed the lowest response amplitudes because this configuration introduced a lower amount of distortion into the inlet flow field compared to the $-30°$ configuration.

The maximum strain amplitudes were reached with a combination of the highest inlet pressure, at $-30°$ *IGV* angle and for *OL*1. The lowest response amplitudes were measured for the lowest inlet pressure at *OL*3 with the $-45°$ inlet guide vane setting.

The highest damping ratios were obtained at highest inlet pressure for $\gamma = -45°$ at *OL*1 whereas the lowest critical damping ratios were estimated for the 0° *IGV* angle at the operating point near stall (*OL*3) with the lowest inlet pressure, as expected.

$\frac{\zeta_{A,ref}}{\zeta_M}\left(\frac{p}{p_{ref}}\right)$	**OL1**	**OL2**	**OL3**
0° **IGV**	1.61	1.53	1.42
$-30°$ **IGV**	2.63	1.88	1.51
$-45°$ **IGV**	2.71	2.19	2.08

TABLE 1. Slope of the Evolution of Aerodynamic Damping Relative to the Material Damping as a Function of the Inlet Pressure

Table 1 summarizes the measured configurations with their corresponding evolutions of the aerodynamic damping ratios as a function of the inlet pressure. As can be seen from equation 12, the values show the slopes of the characteristic curves that are shown in figures 12 and 14. The slopes decrease with decreasing mass flow rates from *OL*1 to *OL*3 and increase for larger negative inlet guide vane angles. An increase in the slope of the characteristics indicates that there is a higher sensitivity of the contribution of aerodynamic damping relative to the overall damping ratio on the inlet pressure setting. The largest sensitivity at *OL*1 with an *IGV* angle of $-45°$ is 1.7 times higher than the sensitivity at the 0° setting for *OL*3 close to stall. The steepness of the sensitivity therefore seems to be influenced by the flow velocity at the inlet of the compressor stage; this hypothesis has to be assessed in ongoing analysis of measurement data.

SUMMARY AND CONCLUSIONS

The damping estimation during forced response blade vibration for a centrifugal compressor with variable inlet guide vanes was performed on the basis of experimental data. The experimental approach allowed the quantification of the strain response and the separation of the contributions from aerodynamic damping and material damping to the overall damping.

Measurements were performed for a number of inlet pressure settings from 200 mbar to 800 mbar absolute. Material damping was calculated from an extrapolation to vacuum conditions. As the present work focused on the resonant response for main blade mode 1 the mode-dependent material damping was assumed to be constant. The measurements showed a linear increase of the aerodynamic damping with increasing inlet pressure as the aerodynamic damping scales with the density. The strain amplitudes during resonant response also showed an inlet pressure dependency, as the unsteady blade load scales with the density. The response characteristics showed an asymptotic approximation with increased inlet pressure to a point where the contribution from material damping to the overall damping could be ignored. At 1 bar the aerodynamic damping typically was higher than the material damping for blade mode 1 by a factor of 3.

It is clear that the damping estimation must be performed under engine representative operating conditions as the compressor operating point and the specific distortion pattern in the inlet flow field directly affect the magnitude of the aerodynamic damping relative to the overall damping properties of the impeller main blades. Furthermore, the compressor operating point and *IGV* angle setting affects the slope of the characteristic increase of the contribution from aerodynamic damping to the overall damping ratio as a function of the compressor inlet pressure setting.

The investigation of the influence of the *IGV* angle on the response amplitudes and damping ratios showed an increase in the damping ratios with increasing blade angles γ. However, the strain amplitudes did not show a similar trend. The response amplitudes were highest for the $-30°$ and lowest for the $-45°$ configuration. The reason for the lower vibratory response levels was a significant relative reduction of the inlet flow non-uniformity for the $-45°$ caused by enhanced mixing and the longer flow path of the swirling flow from the *IGV* plane to the impeller inlet. The detailed investigation of the forcing function is presented in Part 2 of this two-part publication.

The experiments were performed at three different operating points from near-choke to near-stall. The aerodynamic damping decreased with the increased total pressure ratio. However, the strain levels were about 40% higher for the near-choke operating point compared to the other two operating points. The stronger forcing for this operating point is presented in Part 2.

ACKNOWLEDGEMENTS

The authors gratefully acknowledge the intellectual and financial support of their industrial partners ABB Turbo Systems Ltd. and MAN Diesel & Turbo Schweiz AG in this project. The contributions by Dr. Janpeter Kuehnel and Dr. Matthias Schleer from ABB Turbo Systems Ltd. and Mr. Yves Bidaut from MAN Diesel & Turbo Schweiz AG are greatly acknowledged. The authors also acknowledge the financial support provided by the Swiss Confederation's innovation promotion agency, CTI.

REFERENCES

[1] El-Aini, Y., deLaneuville, R., Stoner, A., and Capece, V., 1997. "High cycle fatigue of turbomachinery components - industry perspective". In 33rd AIAA/ASME/SAE/ASEE Joint Propulsion Conference, Vol. AIAA 97–3365.

[2] Kielb, R. E., 1998. "Unsteady flows: An aeroelastic blade design perspective.". In ERCOFTAC Turbomachinery Seminar and Workshop.

[3] Srinivasan, A. V., 1984. "Vibrations of bladed-disk assemblies - a selected survey". *Journal of Vibration, Acoustics, Stress and Reliability in Design,* ***106***, pp. 165–168.

[4] Srinivasan, A. V., 1997. "Flutter and resonant vibration characteristics of engine blades". *Journal of Turbomachinery-Transactions of the ASME,* ***119***, pp. 741–775.

[5] Srinivasan, A. V., Cutts, D. G., and Sridhar, S., 1981. Turbojet engine blade damping. Tech. Rep. NASA-CR-165406, NASA.

[6] Crawley, E. F., 1983. "Aerodynamic damping measurements in a transonic compressor". *Journal of Engineering for Power,* ***105***, pp. 575–584.

[7] Manwaring, S. R., and Fleeter, S., 1990. "Inlet distortion generated periodic aerodynamic rotor response". *Journal of Turbomachinery-Transactions of the ASME,* ***112***(2), pp. 298–307.

[8] Manwaring, S. R., and Fleeter, S., 1991. "Forcing function effects on rotor periodic aerodynamic response". *Journal of Turbomachinery-Transactions of the ASME,* ***113***(2), pp. 312–319.

[9] Manwaring, S. R., Rabe, D. C., Lorence, C. B., and Wadia, A. R., 1997. "Inlet distortion generated forced response of a low-aspect-ratio transonic fan". *Journal of Turbomachinery-Transactions of the ASME,* ***119***(4), pp. 665–676.

[10] Manwaring, S. R., and Wisler, D. C., 1993. "Unsteady aerodynamics and gust response in compressors and turbines". *Journal of Turbomachinery-Transactions of the ASME,* ***115***(4), pp. 724–740.

[11] Haupt, U., and Rautenberg, M., 1984. "Blade vibration measurements on centrifugal compressors by means of telemetry and holographic-interferometry". *Journal of Engineering for Gas Turbines and Power-Transactions of the ASME,* ***106***(1), pp. 70–78.

[12] Jin, D., 1990. *Untersuchung von Schaufelschwingungen und ihrer Erregungsursachen an Radialverdichtern*. Dissertation. Hannover.

[13] Kielb, J. J., and Abhari, R. S., 2003. "Experimental study of aerodynamic and structural damping in a full-scale rotating turbine". *Journal of Engineering for Gas Turbines and Power-Transactions of the ASME,* ***125***(1), pp. 102–112.

[14] Kammerer, A., and Abhari, R. S., 2009. "Experimental study on impeller blade vibration during resonance Part 1: Blade vibration due to inlet flow distortion". *Journal of Engineering for Gas Turbines and Power,* ***131***(2), pp. 022508–11.

[15] Kammerer, A., and Abhari, R. S., 2009. "Experimental study on impeller blade vibration during resonance Part 2: Blade damping". *Journal of Engineering for Gas Turbines and Power,* ***131***(2), pp. 022509–9.

[16] Abhari, R. S., and Giles, M., 1997. "A navier-stokes analysis of airfoils in oscillating transonic cascades for the prediction of aerodynamic damping". *Journal of Turbomachinery - Transactions of the ASME,* ***119***(1), pp. 77–84.

[17] Silkowski, P. D., and Hall, K. C., 1998. "A coupled mode analysis of unsteady multistage flows in turbomachinery". *Journal of Turbomachinery - Transactions of the ASME,* ***120***(3), pp. 410–421.

[18] Dickmann, H. P., Wimmel, T. S., Szwedowicz, J., Filsinger, D., and Roduner, C. H., 2006. "Unsteady flow in a turbocharger centrifugal compressor: Three-dimensional computational fluid dynamics simulation and numerical and experimental analysis of impeller blade vibration". *Journal of Turbomachinery-Transactions of the ASME,* ***128***(3), pp. 455–465.

[19] Zemp, A., Schleer, M., and Abhari, R. S., 2011. "Experimental investigation of forced response impeller blade vibration in a centrifugal compressor with variable igvs – part 2: forcing function and fsi computations". In ASME Turbo Expo, Vol. GT2011–46290.

[20] Schleer, M., 2006. *Flow structure and stability of a turbocharger centrifugal compressor*. Dissertation ETH Nr.

16605. VDI-Verlag, Düsseldorf.
[21] Traupel, W., 1982. *Thermische Turbomaschinen*. Springer. Berlin.
[22] Kassens, I., and Rautenberg, M., 1998. "Flow measurements behind the inlet guide vane of a centrifugal compressor". *ASME Paper, 98-GT-86*.
[23] Lenherr, C., Kalfas, A., and Abhari, R. S., 2011. "High temperature fast response aerodynamic probe". *Journal of Engineering for Gas Turbines and Power, **133***(1).
[24] Ewins, D. J., 2000. *Modal testing theory, practice and application*, 2nd ed. Research Studies Press, Baldock, Hertfordshire, England.
[25] Szwedowicz, J., Senn, S. M., and Abhari, R. S., 2002. "Optimum strain gage application to bladed assemblies". *Journal of Turbomachinery-Transactions of the ASME, **124***(4), pp. 606–613.
[26] Craig, R. R., and Kurdila, A. J., 2006. *Fundamentals of structural dynamics*, 2nd ed. John Wiley, Hoboken, NJ.